Modelling of the Time-Dependent Atmospheric Tradewind Boundary Layer with Non-Precipitating Cumulus Clouds *

Ernst Augstein and Melchior Wendel

Max-Planck-Institut für Meteorologie, Hamburg

(Manuscript received 26.11.1979, in revised form 6.6.1980)

Abstract:

The observed multilayered thermodynamic vertical structure of the atmospheric boundary layer of the undisturbed maritime tradewind flow is simulated by a one-dimensional numerical model. The vertical cloud transports of dry sWjc energy and of water mass ar® parameiterized under the assumption of a height-independent vertical cloud mass temsport throughout Sh® büöyart regime of the cloud. tayer. A lateral mass exchange between the model cloud and its environment is taken into account by an empirical function.

The numerical investigations based on measurements during the Atlantic Tradewind Experiment 1969 (ATEX) show that the diurnal Variation of solar radiation causes a convective cycle of the same period which significantly Controls the height of the atmospheric boundary layer.

The vertical extension of the mixed layer seems to be mainly governed by the thermodynamic state of the subcloud layer air. We find that the lifting condensation level of the air at 10 m height in the model agrees closely with the observed top of the mixed layer.

Radiation is found to be of equivalent influence on the boundary layer development as the large scale vertical subsidence and the horizontal advection of heat and water vapour.

Zusammenfassung: Modellsimulation der zeitabhängigen Passat-Grenzschicht mit nichtregnenden Cumuluswolken

Der m dar ungestörten maritim an PassatStrömung beobachtete mehrschichtige Vertikalaufbau der atmösphäriscjien Grenzschicht wird mit Hilfe eines eindimensionalen Modells nachgebliefet. Die Vertikaltrunsporte von trockenstatischer Energie und Wassermasse durch Cumuluswolken werden unter der Annahme eines höhenkonstanten Wölkenmassenfhisscs im Auftriebsbereich parameterisiert. Ein lateraler Massenaustausch zwischen der Modellwolke und ihrer Umgebung wird mittels einer empirisch festgelegieii Punktion berücksichtigt.

Die sich auf Messungen des Atlantischen Passat-Experiments 1969 (ATEX) gründenden numerischen Untersuchungen erbringen, daß der Tagesgang der solaren Einstrahlung einen gleichperiodischen Konvektionszyklus hervorruft, der erheblichen Einfluß auf die Höhe der Grenzschicht nimmt.

Die vertikale Ausdehnung der durchmischten Schicht scheint im wesentlichen von dem thermodynamischen Zustand der Luftmasse zwischen Meeresoberfläche und Wolkenbasis abzuhängen. Denn wir erhalten das Resultat, daß das Hebungskondensationsniveau der Luft in 10 m Höhe gut mit der gemessenen Obergrenze der durchmischten Schicht übereinstimmt.

Die StahilUiHgsfliiß'divitegcn?. übt auf die **Entwicklung der** Grenschicht einen der mittleren Absinkbewegung und der Horizontaladvektion von Wunne und. Watöeidampf vergleichbaren Einfluß aus.

Resume: Un modele de la couche-limite des alizes, dependant du temps, avec des cumulus sans precipitations

On simule par un modele numerique unidimensionnel la structure verticale observee, ä plusieurs couches, de la COUchS'limitßahnospherique däns je courant alfeiS maritimic non perturbe. Les transports verticaux d'energie statique .jBlc'hie"' et de mässe d'eau par les cumulus-sont parametrises moyennant l'hypothese d'un transport do mässe indcpendanl dc .r&'ltitude dans Iß partie convective de la couche nuageuse. On represente par une fonction empirique un echange lateral de mässe entre le nuage et son environnement.

Les recherches numeriques basees sur des mesures de l'„Experience de l'Alize Atlantique (ATEX)" de 1969 montrent que la Variation diurne du rayonnement solaire provoque un cycle convectif de meme periode, qui influence de faijon significative la hauteur de la couche-limite atmospherique.

* Dedicated to Prof. Dr. H. Riehl on the occasion of his 65th birthday

0005-8173/80/04 0509-30 $ 02.00/0

L'extension verticale de la couche de melange semble gouvernee principalement par l'etat thermodynamique de la couche d'air sous le nuage. On trouve que le niveau de condensation par soulevement de I'air ä 10 m de hauteur concorde avec le sommet observe de la couche de melange.

La subsidence a grande echelle et l'advection horizontale de chaleur et de vapeur d'eau apparaissent comme ayant une influence equivalente ä celle du rayonnement sur le developpemept de la couche-limite.

List of Symbols

Symbol	Units	Explanation
a	undetermined	variable quantity
ä, b̂, c, e_c	K d^{-1}	empirical constants in radiation formula
d̂	K d^{-1} m^{-1}	
c_p	J g^{-1} K^{-1}	specific heat at constant pressure
C_H> C_E	—	transfer coefficients for turbulent fluxes of sensible and latent heat, respectively
k	—	System parameter of the model
ß	kg kg^{-1}	liquid water content of air
P	kg m^{-1} s^{-2}	pressure
q	kg kg^{-1}	specific humidity of air
q_s	kg kg^{-1}	Saturation specific humidity of air
s	J g^{-1}	dry static energy of air
t	s(d)	time
lül$_{10}$	m s^{-1}	wind speed at 10 m height
w	m s^{-1}	vertical component of motion
z	m	vertical distance from sea surface
$\bar{z}_m$	m	height of the mixed layer
$\bar{z}_b$	m	cloud base
$\bar{z}_{en}$	m	height of level of non-buoyancy of cloud air
$\bar{z}_{db}$	m	top of active cloud layer
$\bar{z}_{dt}$	m	top of passive cloud layer
A_o z	m	(z_{cn} - Zdb) at time t = 0
Fso	W m^{-2}	sensible heat flux at the sea surface
Fqo	W m^{-2}	latent heat flux at the sea surface
F®vo	W m^{-2}	buoyancy flux at the sea surface
L	J g^{-1}	latent heat of evaporation and condensation
LCL_{10}	m	lifting condensation level of air at 10 m height
R	W m^{-2}	radiative flux
T	K	temperature
a,ß	m^{-1}	coefficients
ö	s^{-1}	lateral exchange rate
5*	m^{-1}	lateral exchange coefficient

φ	h	time phase lag with respect to GMT
p	kgm^{-3}	air density
a	%	relative area covered with active clouds
r_s, r_q	—	profile coefficients of s and q
Θ	K	potential temperature
Θ_v	K	virtual potential temperature
$\bar{\varrho}_c^*$	kg kg^{-1}	liquid water content
$\bar{q}_c^*$	kg kg^{-1}	specific humidity
$\bar{q}_{\varrho c}^*$	kg kg^{-1}	total water content
$\bar{s}_c^*$	Jg^{-1}	dry static energy
$\bar{s}_{\varrho c}^*$	J g"*	dry static energy including effects of phase changes of water
$\bar{w}_c^*$	m s^{-1}	vertical motion
$\bar{\Theta}_{v\varrho c}^*$	K	liquid water virtual potential temperature

Subscripts o, 10, z_m, z_b, Zj_b, Zd_t refer to sea surface, 10 m height, top of the mixed layer, cloud base, top of active cloud layer and top of the passive cloud layer, respectively. Subscripts m and c identify mixed layer and cloud properties, respectively.

Overbar indicates horizontal averages and tilde marks vertical layer averages. Primed values are local deviations from the horizontal mean. Asterisks symbolize model cloud properties.

1 Introduction

Observations at various oceanic sites in low latitudes support the view that a multilayered thermodynamic structure, as first described in detail by BUNKER et al. (1949) for the Caribbean Sea, is characteristic of a major part of the tradewind flow in the lower troposphere. Budget studies by e.g. HOLLAND and RASMUSSON (1973), AUGSTEIN et al. (1973), RIEHL and SOLTWISCH (1974) and BRUEMMER (1976) all show that the vertical, turbulent and convective sensible and latent heat fluxes, and the frictional influence of the sea surface on the mean air stream more or less terminate at the socalled tradewind inversion. Consequently, we shall specify the atmospheric region below the top of the tradewind inversion as the atmospheric boundary layer (ABL).

In the core regime of the Hadley cell, between the subtropical high pressure beit and the Intertropical Convergence Zone (ITCZ), non-precipitating cumulus clouds appear to be a significant phenomenon in the upper part of the ABL. RIEHL et al. (1951) have already stated that the bases for this type of clouds are roughly uniform in height, while their tops considerably differ in altitude. The most active members of the cloud ensemble reach up into the inversion layer. Occasionally, the inversion is even penetrated by very intense cumuli, but such conditions will not be considered in this paper..

Measurements of the vertical thermodynamic structure clearly demonstrate distinct changes in the mean vertical temperature and water vapour profiles near the cloud base. A relatively thin, statically stable transition layer (50—150 m) separates a well mixed subcloud regime from the cloud layer above. Acknowledging the fact that some clouds extend into the tradewind inversion, and that cloud transports are extremely important for the maintenance of this layer, we will consider the inversion to be a part of the cloud layer and refer to it as the „passive cloud layer" in the subsequent discussion.

Measurements of various investigations such as those published by KUHLBRODT and REGER (1933), RIEHL et al. (1951), MALKUS (1958), NEIBURGER et al. (1961), NITTA and ESBENSEN (1974) and

AUGSTEIN et al. (1974) document the fact that the layered structure of the tradewind ABL may considerably vary in space and time. Reasonable qualitative explanations for such changes have already been offered by RIEHL et al. (1951), MALKUS (1958) and KRAUS (1963), among others, but the effect of e.g. a given modification in the large-scale field or the radiative flux on the processes and final state of the boundary layer is still uncertain.

In order to increase our insight into these interrelationships, we shall attempt to simulate the time development of the multilayered tradewind boundary layer with non-precipitating cumulus clouds through the use of a one-dimensional numerical model. Data obtained during the Atlantic Tradewind Experiment ATEX in 1969 will be used to guide and verify the computations in this study. Our numerical concept is principally an extension of the mixed layer models of BALL (1960), LILLY (1968), CARSON (1973), TENNEKES (1973), DEARDORFF (1976) and others. In order to include cumulus clouds into the computations we alter the assumption that small-scale mixing, from below, does not penetrate the top of the stable jump region, which caps the mixed layer. Instead, we imply that some parcels move further upwards and reach their condensation level. Our approach does not consider the generation of cumulus clouds which has been studied recently by MAHRT (1979), but we assume that non-precipitating clouds are continuously present.

On the basis of similar prerequisites this kind of boundary layer was first treated by BETTS (1973), who used an entraining, vertically moving cloud parcel to parameterize the non-precipitating cumulus clouds within the regime above the mixed layer. With the aid of this principle, he was able to achieve a reasonable description of the influence of clouds on the thermal stratification of the cloud layer. However, he did not consider the convective water vapour transports explicity, which are presumably even more important in the formation and maintenance of the ABL structure.

Rather comprehensive studies of the tradewind ABL sketched above, which also include momentum equations, have been conducted by SOMMERIA (1976), and SOMMERIA and DEARDORFF (1977) with the use of a three-dimensional model. The advantage of their approach is that it resolves clouds above a certain size explicitly and parameterization is only required for the smaller turbulence scale. Unfortunately, it has rather high computational demands so that its application is restricted to the treatment of short time periods. Promising new one-dimensional schemes for the prognostic study of an atmospheric boundary layer with non-precipitating cumulus clouds have recently been advanced by JOHNSON (1978) and ALBRECHT et al. (1979). In both of their investigations, as well as in this model, the effect of cloud transports on the ABL structure is parameterized in terms of a vertical cloud mass flux. On the basis of the equation of continuity for the model clouds, the vertical convective flow and the lateral mass exchange between the cloud ensemble and the cloud free environment is represented by a simple parameterization scheine. Our model differs from the two just mentioned in the detailed treatment of the vertical cloud mass flux, the lateral mass exchange between the clouds and their environment, and in the determination of the top and base of the cloud layer.

In order to achieve a closed set of model equations, a number of simplifying assumptions and some empirical coefficients must be introduced. Among the empirical parameters, one may distinguish between those which are externally prescribed and those which can be freely chosen. The first ones take on the meaning of universal constants, in the framework of this model's considerations, while the later ones can be adjusted so that the model results satisfactorily fit the observed data. It is easy to convince oneself that as the number of free model parameters grows, the degree of fitting increases and the uniqueness of the numerical calculations decreases. But since we are primarily interested in the principle influence of various processes on the development of the ABL, rather than in the Simulation of all details of specific cases, we have tried to construct a model scheme with only two free parameters.

Our concept is briefly sketched in the subsequent paragraph. Then, the sensitivity of the model, with respect to the choice of free parameters, is considered. Finally , the application of the numerical scheme to the mean diurnal Variation and to an undisturbed 7-day period of ATEX is presented.

2 The Model Concept

2.1 The Vertical Structure of the Model

The model regime vertically extends from the sea surface to a height of 2500 m, well above the top of the atmospheric boundary layer during ATEX. In qualitative agreement to measurements, the entire vertical region is subdivided into six different layers as portrayed in Figure 1.

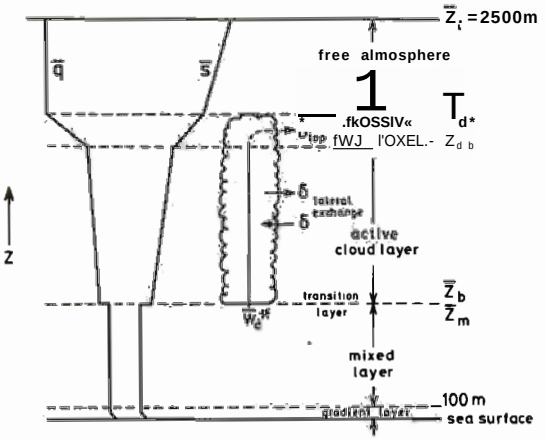

® **Figure 1**
Schematic structure of the model ABL. q = specific humidity, s = dry static energy, w£ = cloud motion, 5 = lateral mass exchange parameter

• **Bild 1**
Schematischer Aufbau der Modellgrenzschicht. $\bar{q}$ = spezifische Feuchte, s = irpcker.statische Energie, Wc = Wolkenbewegung, *6* = literalw Massenaustausch-parameter

The mean dry static energy $\bar{s} = c_p \bar{T} + g\bar{z}$ and the mean specific humidity $\bar{q}$ are expressed by a logarithmic profile in the gradient layer below 100 m height. Both quantities are taken as height independent in the mixed layer, and they form a jump in the infmitesimally thin transition layer. Linear changes of s and q with height are assumed within the active and passive cloud layers. Throughout the free atmosphere, the specific humidity assumes its upper boundary value while the dry static energy again forms a linear vertical profile. On the basis of these assumptions, the model predicts s and q at a height of 10 m within the mixed layer, at the levels z_b , za_b and zj_t , as well as the heights of $z_m = z_b$ and of zj_b . The initial vertical profiles and boundary values of s and q at the sea surface and at 2500 m must be specified externally. The height difference (zj_t - za_b) is assumed to be time independent and therefore given by the initial profiles of $\bar{s}$ and $\bar{q}$.

In the calculations, the natural cloud ensemble is represented by one single type of model cloud with a top-hat-like profile, which is similar to that proposed by YANAIet al. (1973). The lower region of the cloud layer, where this model cloud is positively buoyant, is called the "active cloud layer". The upper part (the Inversion), where the upward forced cloud mass is negatively buoyant, is called the "passive cloud layer". In contrast to YANAIet al. (1973), but in agreement with FRAEDRICH(1974), we assume that the model cloud mass flux wj is independent of height throughout the entire active layer, and that it decreases to zero within the passive layer. Thermodynamic interaction between the clouds and their environment is achieved by a lateral mass exchange across the vertical surface of the model cloud. According to the mass flux scheme within the active sublayer, the entrainment of ambient air into the cloud must be fully balanced by detrainment of cloud matter into the environment. In the passive sublayer, the cloud gradually dissolves and its mass is diffused into the mean flow. The height dependent function of lateral

Our concept is briefly sketched in the subsequent paragraph. Then, the sensitivity of the model, with respect to the choice of free parameters, is considered. Finally , the application of the numerical scheme to the mean diurnal Variation and to an undisturbed 7-day period of ATEX is presented.

2 The Model Concept

2.1 The Vertical Structure of the Model

The model regime vertically extends from the sea surface to a height of 2500 m, well above the top of the atmospheric boundary layer during ATEX. In qualitative agreement to measurements, the entire vertical region is subdivided into six different layers as portrayed in Figure 1.

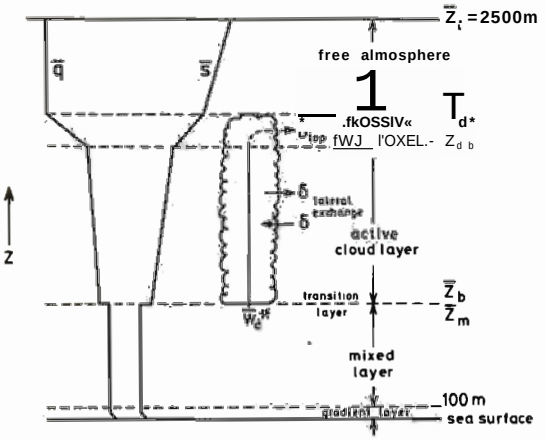

® **Figure 1**
Schematic structure of the model ABL. q = specific humidity, s = dry static energy, w£ = cloud motion, 5 = lateral mass exchange parameter

• **Bild 1**
Schematischer Aufbau der Modellgrenzschicht. $\bar{q}$ = spezifische Feuchte, s = irpcker.statische Energie, Wc = Wolkenbewegung, *6* = literalw Massenaustausch-parameter

The mean dry static energy $\bar{s} = c_p \bar{T} + g\bar{z}$ and the mean specific humidity $\bar{q}$ are expressed by a logarithmic profile in the gradient layer below 100 m height. Both quantities are taken as height independent in the mixed layer, and they form a jump in the infmitesimally thin transition layer. Linear changes of s and q with height are assumed within the active and passive cloud layers. Throughout the free atmosphere, the specific humidity assumes its upper boundary value while the dry static energy again forms a linear vertical profile. On the basis of these assumptions, the model predicts s and q at a height of 10 m within the mixed layer, at the levels z_b , za_b and zj_t , as well as the heights of $z_m = z_b$ and of zj_b . The initial vertical profiles and boundary values of s and q at the sea surface and at 2500 m must be specified externally. The height difference (zj_t - za_b) is assumed to be time independent and therefore given by the initial profiles of $\bar{s}$ and $\bar{q}$.

In the calculations, the natural cloud ensemble is represented by one single type of model cloud with a top-hat-like profile, which is similar to that proposed by YANAIet al. (1973). The lower region of the cloud layer, where this model cloud is positively buoyant, is called the "active cloud layer". The upper part (the Inversion), where the upward forced cloud mass is negatively buoyant, is called the "passive cloud layer". In contrast to YANAIet al. (1973), but in agreement with FRAEDRICH(1974), we assume that the model cloud mass flux wj is independent of height throughout the entire active layer, and that it decreases to zero within the passive layer. Thermodynamic interaction between the clouds and their environment is achieved by a lateral mass exchange across the vertical surface of the model cloud. According to the mass flux scheme within the active sublayer, the entrainment of ambient air into the cloud must be fully balanced by detrainment of cloud matter into the environment. In the passive sublayer, the cloud gradually dissolves and its mass is diffused into the mean flow. The height dependent function of lateral

exchange across the vertical cloud surface 8 between z_b and z_{db} represents one of the two free System Parameters. The second one is the turbulent mixing factor k. It specifies the portion of buoyancy generated turbulent kinetic energy, which is converted into potential energy through downward turbulent and convective transports of lower potential density air across the top of the mixed layer. This coefficient k was first introduced into the budget equation of turbulent kinetic energy by LILLY (1968). In our approach, this equation will be applied to determine the vertical motion of the model cloud $\bar{w}j$.

2.2 The Model Equations

The mathematical treatment of the trade wind boundary layer is based on the simplified budget equations of dry static energy $s = c_p T + gz$ and specific humidity q in the following form:

$$\frac{\partial s}{\partial t} = -\bar{w}\frac{\partial s}{\partial z} - \frac{\partial \overline{(w)}}{\partial z} + \frac{1}{\rho}\frac{\partial R}{\partial z} + (\bar{C} - \bar{E}) + \bar{s}_{adv} \qquad (1)$$

$$\frac{\partial q}{\partial t} = -\bar{w}\frac{\partial q}{\partial z} - \frac{\partial \overline{(w\,q')}}{\partial z} + \frac{1}{L}(\bar{C} - \bar{E}) + q_{adv} \qquad (2)$$

Variations of the mean density with respect to height are neglected. The overbars indicate horizontal averages and the primes mark local deviations from these averages. We choose the common notations as: ρ = air density, w = vertical component of velocity, R = radiative flux, C = condensation of water vapour, E = evaporation of liquid water, L = latent heat of condensation and evaporation, t = time and z = vertical coordinate. s_{adv} and q_{adv} symbolize the horizontal advection of dry static energy and specific humidity due to the mean flow. Since the latter quantities are taken into account, we must admit that the model is not purely one-dimensional.

Equations (1) and (2) will be solved as a combined initial-, boundary-value problem for vertical averages of s and q over (a) the combined gradient and mixed layer, (b) the active cloud layer, (c) the passive cloud layer, and (d) the region between the top of the cloud layer and the upper boundary of the model at 2500 m height. The mean flow properties of large scale subsidence $\bar{w}$ and horizontal advection $_{adv}$ and q_{adv} must be specified externally, as well as the boundary conditions at the sea surface z_0 and at the upper boundary $z_t = 2500$ m.

Through the vertical Integration of Equations (1) and (2), the levels $z_m = z_b$ and $z_{dt} = z_{db}$ + const appear as additional unknowns in the System. Therefore, two more independent equations are required for Solution. Suitable formulae are also necessary to determine the primed perturbation fluxes — which include turbulent and cloud transports — and the radiative fluxes at the various horizontal layer boundaries, and to specify condensation and evaporation in both subregions of the cloud layer.

A closed set of equations is finally obtained with the aid of the following assumptions:

a) At the sea surface:

For the turbulent fluxes at the sea surface, the aerodynamic bulk formulae are applied:

$$(w's')_0 = c_h(s_0 - s_{10})\,|\bar{u}|_{10} = |f_{so} \qquad (3)$$

$$(w'q')_o = c_E\,(Q_{so} - Q_{io})\,|\bar{u}|_{10} = F_{qo} \qquad (4)$$

In Equations (3) and (4) Ch and c_E represent the turbulent transfer coefficients for heat and water vapour, respectively. $|\bar{u}|$ is the mean wind speed. The subscripts o, 10, and s in this paper indicate values at the sea surface, at 10 m height, and Saturation in regard to water vapour, respectively. The mean wind speed

lü iio and the sea surface value of dry static energy s_0 must be prescribed. Neglecting temporal air pressure changes, the Saturation value of specific humidity is determined with the aid of the Goff-Gratsch formula (LIST,1956). The dry static energy s_{10} and the specific humidity q_{10} at 10 m height are obtained from the logarithmic profile relationships:

$$\frac{dl}{3z} \sim \frac{\bar{s}_{io} - \bar{s}_o}{z} \tag{5}$$

and

$$\frac{9q}{dz} \sim \frac{\bar{Q}io - \bar{q}o}{z} \tag{6}$$

with the so called profile coefficients $T_s = 0.08$ and $r_q = 0.07$. The numerical values of these coefficients have been determined by KRUEGERMEYER (1975) from ATEX buoy measurements. Under the assumption that at the 100 m level the logarithmic distribution has gradually changed over into the mixed layer values, vertical Integration of Equations (5) and (6) from 10 m to 100 m yields:

$$\frac{\tilde{s}_m + 0.18\ s_0}{L18} \tag{7}$$

and

$$\frac{0.16\ q_{s0}}{1.16} \tag{8}$$

The tilde marks layer averages and the subscript m indicates mixed layer values.

b) At the top of the mixed layer:

In accordance with the observed close correlation between the lifting condensation level (LCL) of surface air and the height of the mixed layer during ATEX (AUGSTEIN,1976), we formulate:

$$z_m = LCLio \tag{9}$$

as a diagnostic equation for the mixed layer height. Variations of the lifting condensation level of air at 10 metres (LCL_{10}) are primarily caused by s_{10} and q_{10} and to a much lesser degree by the vertical distribution of air pressure. Therefore, in our case the latter is prescribed by a mean stationary profile.

According to Equation (9) and the prerequisite that the cloud base z_b and the mixed layer height z_m coincide in the model ABL, the approximate cloud properties at z_b are consistently given by:

$$\$cz_b \sim Sio> \qquad 9cz_b \sim qio, \qquad \bar{\ }cz_b \_0. \tag{10}$$

The subscript c indicates cloud properties, and ß means the liquid water content in $kg \cdot kg^{-1}$.

Assuming that all particles, which distinctly penetrate the transition jump atop the mixed layer become cloud matter at the cloud base z_b, the following perturbation fluxes are obtained for this level:

$$(w's')_{zb} = Wo(s_{10} \sim s_{zb}) \tag{11}$$

and

$$\overline{(w'q')z_b} = w*(qio - qz_b) \tag{12}$$

The quantity $\bar{w}$<J marks the vertical motion within the model cloud.

In order to determine w£, we integrate BALL's (1960) highly simplified Version of the turbulent kinetic energy equation from the sea surface z_0 to the top of the mixed layer z_m. This is done on the assump-

tion thät the buoyancy flux at cloud base, which results from the transports given by Equations (11) and (12), does not vanish. Additionally introducing the mixing factor k we obtain:

$$\text{™}c(\overline{®v_{10}} \sim {}^{0}\overline{vz_b}) + \frac{dz_m}{\text{ud}}\text{----}w_{Zm}\ (\overline{€>v_m} - \overline{®vz_b})^{+}\ k(\overline{w'0;})o = O \tag{13}$$

The virtual potential temperature 0_V results, with sufficient accuracy, from

$$0_V \quad \frac{1}{c_p}\ s(1 + 0.608\ q) \tag{14}$$

The mean vertical motion $\overline{w}_{Zm}$ at z_m is a prescribed property and the buoyancy flux at the sea surface $(w'0y)_o$ results from the approximate relationship:

$$(\overline{w'0Oo} \quad \frac{1}{p}\ \{(\overline{w's'})_0 + 0.608\ s_{10}\ (\overline{w'q'})_0] \tag{15}$$

The parameter $0 < k < 1$ accounts for the dissipation of buoyancy generated turbulent kinetic energy within the layer below z_m. Taking $k = 1$ and $\overline{w}j = 0$, Equation (13) is identical to BALL's(1960) turbulent kinetic energy equation.

The preceding approach is only valid if the mixing processes at the top of the mixed layer are dominantly forced by buoyancy generated turbulence from below. Radiative effects as considered by e.g. LILLY (1968), DEARDORFF(1976), KRAUS and SCHALLER(1978), and KAHN and BUSINGER(1979) are probably negligibly small in our case, since neither stratiform clouds nor haze appear near the top of the layer. According to TENNEKES(1973) and STULL(1976) mechanically generated turbulence may also contribute to the mixed layer development and consequently influence the cloud mass flux. But in the ATEX Situation the observed small values of vertical wind shear in the transition layer more or less exclude any significant turbulence production by breaking internal waves. Nvertheless, some uncertainly still remains in our model scheme since a part of the turbulent kinetic energy created by the work of stress on the mean shearing flow, particularly near the sea surface, may be transported upwards and participate in the actual mixing at the top of the mixed layer.

c) Within the cloud layer:

Within our formal scheme influences of the above cloud layer on the mixed layer occur through the mean quantities of dry static energy, specific humidity, and virtual potential temperature at cloud base z_b. These values are not only dependent upon radiation and variations of the large scale field, but are also affected by the cloud process, which roots down into the mixed layer. Consequently, s and q at cloud base cannot be prescribed externally,but must rather be determined by the model internally. It is this demand which makes the inclusion of the cloud layer into the ABL model necessary, and thereby forces us to describe the cloud process with the aid of an adequate parameterization scheme. For this purpose, we express the approximate horizontal average of the total vertical transport of a property "a" at a given level within the cloud layer by:

$$wa = wa + w'a' \text{«}\ \{uw_c + (1 - a)w_e\}\ddot{a} + o\{w_c(a_c - a) + (w\ ac)\} \tag{16}$$

The first term on the right hand side of Equation (16) represents the flux of the mean motion. It is composed of the average motion of the active cloud area w_c times the fractional coverage of active clouds a and the average environmental motion w_e times the complementary area fraction (1 - u). The second term on the right hand side of the above relationship expresses the perturbation fluxes caused by the mean cloud vertical velocity w_c and by the fluctuations around w_c within the area a. The contribution of turbulence in the cloud free regime to the vertical transports is considered negligibly small according

to aircraft measurements of LeMONE and PENNELL (1975) over the Caribbean Sea. Thus, the horizontally averaged perturbation fluxes of a property "a" may be finally parameterized by:

$$\overline{w'a'}^{ft} = o\{w_c(\ddot{a}_c - \ddot{a}) + \overline{Wcac}\} \quad Wc(\ddot{a}^* - \ddot{a}) \tag{17}$$

The asterisk values again represent horizontal averages of cloud quanties, which are not necessarily identical to observable parameters. As mentioned earlier, the vertical motion in the model cloud $\bar{w}^*$ will be taken as independent of height within the active cloud layer, and as zero at the top of the passive layer. These assumptions are, by and large, in agreement with the aircraft measurements of WARNER (1977), who found a slight increase of $(Wc^2)^{1/2}$ with height, but no significant height variations of w_c for non-precipitating cumulus clouds.

Finally, we imply that the liquid water moves with its original cloud air mass until it is either evaporated inside of the cloud, or detrained and evaporated in the cloud free environment. Under such conditions, $\bar{s}_{\beta c} = s£ - L\beta^*$ and $q_{2c} = q£ + ££$ are conservative cloud properties, and for stationary cloud conditions (i.e.: $\frac{\partial}{\partial t}\bar{s}_{\beta c}^* = \frac{\partial}{\partial t}\bar{q}_{Cr}^* = 0$) we may write:

$$\overline{w_c}\,\frac{\partial(s_{\beta c} - s)}{\partial z} = \frac{\partial \overline{f w' s)}}{\partial z} + (\overline{C} - \overline{E}) \tag{18}$$

$$w \gg \frac{\partial(q_{\ll c} - q)}{\partial z} = \frac{\partial(w'q')}{\partial z} + (C - e) \tag{19}$$

Stationarity of cloud properties may be assumed when the adjustment time of the cloud ensemble to the large scale field is small compared to the temporal changes of the mean quantities. This hypothesis — introduced by ARAKAWA and SCHUBERT (1974) for cloud parameterization — seems to be in sufficient agreement with reality. Making use of Equation (10) under these prerequisites and adding the assumption that the convective and turbulent fluxes are zero at the top of the ABL Zdt, the vertical Integration of the respective budget equations of s_{2c} and qg_c over the active cloud layer leads to:

$$w^* < Sfi_{CZdb} - s_{10}) - \delta(z_{db} - z_m)(S\beta c - s) = 0 \tag{20}$$

$$Wc(q2c_{Zdb} - \bar{q}_{10}) - \tilde{5}(z_{db} - z_m)(\tilde{q}_{2c} - \tilde{q}) = 0 \tag{21}$$

with

$$\tilde{\ell}^*_{CZdb} = -l^{q\beta z}_{db} - {}^{sz}_{db} f^{\circ T} \beta c z_{db} - 4 s e z_{db} \quad \text{for } q_{2c z_{db}} < q^*_{sCZdb} \tag{22}$$

The tilde denotes layer averages, and $\tilde{5}$ (in units of seconds) indicates the rate of lateral mass exchange between the model cloud and its environment. Equation (22) is necessary in order to determine the liquid water content, which will later be needed for the computation of Zdb•

Following TURNER's (1979) concept for the entrainment of mass into a buoyant plume, we will hypothetically introduce a similar relationship for the lateral mass exchange across the boundaries of the model cloud:

$$\ddot{O} = 8^* w^* \tag{23}$$

From computations of a slightly different version of this model, which resolves the cloud layer by a relatively dense vertical grid, AUGSTEIN (1980) finds:

$$5^* = a \exp \beta(z - z_{mo}) \tag{24}$$

with $a = 1.28 \cdot 10^{-3}\ m^{-1}$ and $ß = 7.6 \cdot 10^{-3}\ m^{-1}$ and the mixed layer height at the initial time (t = 0) $z_{mo} = 600$ m. Using these two constants, we can determine the layer averaged lateral mass exchange as:

$$\bar{5} = \frac{\overline{wr}^{*}}{(z_{db} - z_m)} \int_{\bar{z}_m}^{z_{db}} a \exp ß(z - 600)\, dz \qquad (25)$$

This equation will be used for the ATEX calculations with the numerical values for *a* and *ß* quoted above. Since these coefficients represent —in a certain way —the size spectrum of the actual cloud ensemble, one may suspect that they are not universal constants, but rather that they vary with the cloud size distribution. Therefore, it seems not to be admissible to generally reduce the free model parameters to k only through the use of Equation (25). In our specific cases the application of this relationship is justified by the observed small changes of the cloud population.

The height of the top of the active cloud layer z_{db} is specified by the assumption that it is firmly related to the model cloud's level of non-buoyancy z_{cn}. Since the model cloud represents a cloud ensemble instead of a single type of cloud, z_{db} and z_{cn} are not necessarily identical. We, therefore, assume that the relation between these two levels can be approximated by:

$$Zcn = z_d b + A_o z \qquad (26)$$

with $A_o z$ = the difference between the level of neutral buoyancy z_{cn} and the top of the active cloud regime z_{db} at the initial model time t = 0. The value of $A_o z$ is consequently not free for manipulations, but is self-determined during the adjustment procedure of the parameters k and 6. Together with Equation (26), we find z_{db} from the inequalities:

$$\begin{aligned} (®vßc\ “\ ®v)z &> 0 \quad \text{for } z < z_{db} + A_o z \\ (©;_{ec} - 0_V)_Z &< 0 \quad \text{for } z > z_{db} + A_o z \end{aligned} \qquad (27)$$

In Equation (27), the quantity $0^*_{ßc}$ indicates the liquid water virtual temperature of the cloud, which accounts for the liquid water, as well as the water vapour, in the cloud mass density. According to LILLY (1968), $0_v g$ may be defined by:

$$0_{vß} = 0(1 + 0.608\ q\text{-}ß). \qquad (28)$$

d) For radiation:

Finally, the radiative flux divergence must be calculated somehow. This can be principally done with the aid of current radiation schemes such as those applied e.g. by ALBRECHT et al. (1979). Unfortunately, all present radiation models suffer from a considerable uncertainty in the presence of clouds, and they unfavourably require a remarkable computational effort. Therefore, in this study we prefer to describe the radiational flux divergence by the following simple analytical expression, which grossly approximates the mean ATEX conditions treated by AUGSTEIN and WAGNER (1975):

$$\partial K = - \ddot{a} + \dot{b} \log z + 2ff(c + \dot{d}z + e_c) \cos 2ff^{(t - \varphi)} \qquad (29)$$

I II

In Equation (29), Term I represents the mean height dependent radiative cooling, and Term II accounts for diurnal variations. The time t has to be taken in hours referring to GMT, and the height z must be chosen in meters. The layer below 1 m height is not taken into account. The phase difference <*p* between

zero GMT and local noön amoünts to ~ 14 Itours for the ATEX area at about 30 °W longitude. From the ATEX budget ihveStigafiöns, we find theTollowing values for the .coeffiderits:

ä-8.4 and b = 2.4 for I m Az <14Q0m and

a = 0.84 and b = 0 for z > 1400 m

c = 04, e_c - 0 all in units Kd"[1] and d " 0 in nnits Kd"[1] m"[1];

The coefficients d and e_c are not needed for the ATEX cases, but they are nevertheless ädded in order to artifically simulate certäin pössible rädiative effects. The second one allowsus.to üitrpduce a height dependence öf tlie diurnal rädiative heating cyele while the first one may be used tO'accouilt for cloud influences on the rädiative flux divergence. Thelattei, which according to GRASSL(1978) äcts parüculariy in the top region öf the cloud, will be talcen care of by preseribing e_c 0 only in the passive cloud läyer, and e_c = 0 everywliere eise.

On the bäsis öf the assumptions discussed under the previous paragraphs ä) to d) in Illis chaptpr we have förmed ä set of model equations based an Equations (1) to(29) and using the fomxulae for the Saturation specific humidity and the liftlng condensation leyel, as givenin the Snxithsonian Täbles(LIST,1956). In Order to close the system of equations varipus emperical coefficients äre required. Asmcntionfed earlier generally twö of these, namely k and d[!.:], can be freely Chosen while the others are extemally prescribed . Furthermpre, fixe föllowmg quantitiesmust be specified:

a). initial values of ¥ and q,
b) boundary conditiöns ¥q and lü 1_{10} at the lower and si-t and q_{zt} at fixe Upper boundary öf the model,
c) values of the large scale subsidence w,
d) themean horizontal advcction $¥_a d_V$ and $q_{acäv}$,
e) the mean vertical profile of ait pressure p.

The full set of layer iritegräted model equations is compiled in the Appendix. It contäins prognostic equations for.sublayer averages öf J and q, and diagriöstiö equations for all o.ther quantities, which appeär ort the left händ.side of the equations.

2.3 Wumerical Procedure, Initial Valües and Boundary Cönditions

The time Integration.of the model equations outlined in the Appendix is carried out iteratively . The iterätioiiproeeduie is controlled by the vertical clo.ud motion w£ and by the height of the.mixed läyer Z_m . Solutions are achieved acc.ording to the fix ppint method with the aid of the so called Steffensen-procedure (HElNRia, 1972). Satisfactory convergejice in the Iteration is obtained for Integration time Steps At of less.than 120 seconds. For At <120 s, the results areindependerit öf the choice of At wltliirithe frame of needed accuracy. Several detäils of fixe numerical procedura, which significaritly optimize the GpmputatiöiiS, nevertheless haye mainly Technicalitnplicätiöris and will, therefore, not be discussed in conneetion to this;

The .model will be applied to .twö different ATEX data sets, namely .the meän diürnäl Variation of the A13L duringthe 14 days of nxeasurements in the Atlantic NE träde wind region (subsequeritly called·Oase I), and a continuoüs time series of seven days with light to moderate cloud convection in a relatively steady air flow (subsequently called case II). The experimental background and data evaluation of ATEXhas been discussed elsewhere (e.g. AUGSTEIN et al., 1973; and AUGSTEIN and WAGNER,1975) and will, therefore, be omitted here.

The initial conditions of s, q, w, and fixe prescrlbed horizontal advection of static energy and speqific humidity are listed in Table 1. In the model, the large scale subsidence w is approximated with sufficient accuracy by three süpporting pöints. These are* z ==0 at the sea surface, z at the top of-the active

■ Table 1 Initial conditions for the Simulation of the mean diurnal Variation (Case I) and the 7-day time period (Case II) of ATEX. The horizontal advection marked by *) is bound to the passive cloud layer throughout the entire period of Investigation. Dimensions are given in brackets.

■ Tabelle 1 Anfangsbedingungen für die Simulation des mittleren Tagesganges (Case I) und der 7-tägigen Zeitserie (Case II) des ATEX. Die durch *) markierte Horizontaladvektion ist während des gesmaten Untersuchungszeitabschnittes an die passive Wolkenschicht gebunden. Einheiten sind in Klammern angegeben.

level	Case I						Case II					
	height (m)	$\bar{s}$ (Jg“¹)	$\bar{q}$ (gkg ’)	$\bar{w}$ (10’³ ms⁻ʲ)	$\bar{Q}_{adv}$ (s^{-1})	$\bar{s}_{adv}$ (Jg-> S-»)	he'igt (m)	$\bar{3}$ (Jg“¹)	$\bar{q}$ (gkg-¹)	$\bar{w}$ (10^{-3} ms-¹)	$\bar{Q}_{adv}$ (s">)	$\bar{S}_{adv}$ (Jg-'s'¹)
sea surface	0	302.0	—	0	-2.5-IO"⁸	-2.2 10-8	0	300.2	-	0	-1.5-IO"»	- 0.7 - 10"⁵
100 m	100	300.3	15.9	-0.45			100	298.9	14.10	- 0.6		
$\bar{z}_m$	600	300.3	15.9	- 2.8			600	298.9	14.10	- 3.6		
ib	600	301.25	14.6	- 2.8	0	0	600	299.8	12.7	- 3.6	0	0
$\bar{z}_{db}$	1400	302.15	12.6	-6.5			1300	300.5	11.0	- 7.8		
$\bar{z}_{dt}$	1600	305.9	5.0	- 6.1			1500	304.2	5.0	-7.0	0	- 3 IO’⁵ *)
$\bar{Z}t$	2500	306.9	5.0	- 3.0	0	0	2500	305.0	5.0	- 3.0	0	+ 0.25-10⁻⁵

cloud layer, and $z = z_t = 2500$ m at the upper boundary of the model. The values of $\bar{w}$ at the other horizontal boundaries are obtained through linear Interpolation between the levels mentioned above.

For case I, a diurnal oscillation of the large scale subsidence is taken into account, based on the ATEX data by: $w(t) = w - \cos \sin 2\pi(t - 1)/24$ with the amplitude factor $co = 5 \cdot 10^{-7}$ s^{-1}. In this formula, the height z must be introduced in m, and the time t is given in hours of GMT. The phase of this diurnal mode of subsidence roughly agrees with the BOMEX result of NITTA and ESBENSEN (1974), while our amplitude is only half as large as theirs. The time dependence of w during the ATEX case II is satisfactorily approximated by the curve of $\bar{w}_{max}$ in Figure 3. Since observations in the trades show that the height of the maximum large scale subsidence, by and large, coincides with the top of the active cloud layer, the values of w_{max} in Figure 3 are chosen for $\bar{w}$ at the level zjb. The mean downward motion at $z_t = 2500$ m is taken as constant with time.

The large scale horizontal advection of dry static energy and water vapour for the model Simulation is not prescribed from observations, but freely chosen in order to achieve close agreement between the observed and computed values of s and q at the end of the Simulation period. The values in Table 1 not only account for the influence of the actual advection terms, but also compensate for effects on the model budgets, which are caused by several idealizations in the numerical concept (e.g. that no convective fluxes penetrate the top of the passive cloud layer). In spite of this fact, the model and ATEX advection differ by less than 30 % in case I. For case II, agreement between the observed and computed long term behaviour of 's and q in the mixed region and active cloud layer can only be obtained if the model advection for both quantities in Table 1 is about half as large as that derived for ATEX.

With respect to the vertical distribution of horizontal advection, measurements and computations of the two cases are at least qualitatively similar, since both are mainly concentrated on the subcloud layer. During case II, a remarkably high rate of cold air advection in the passive cloud layer is required in the model in contrast to observations. But this cooling compensates for the heat loss of the passive cloud layer which

is caused by an upward small scale heat flux across zjt during the unperturbed ATEX period according to **AUGSTEIN** and **WAGNER** (1975). The positive advection of dry static energy at the level z_t = 2500 m has been observed at two corner points of the ATEX triangle but not at the third one.

The sea surface conditions employed for case I are displayed in Figure 2, and those for case II appear in the lower part of Figure 3. The observed hourly data are linearly interpolated for the individual model

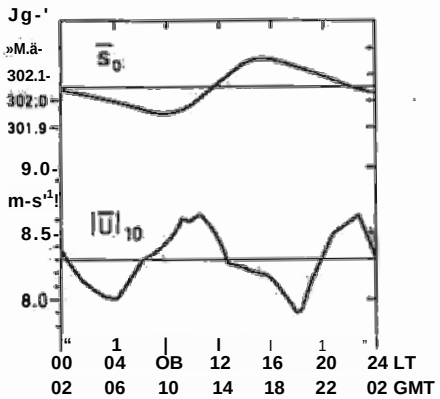

- **Figure 2**
  Lower boundary conditions of case I after PRUEMM (1976). $\bar{s}o$ = dry static energy at the sea surface $l\bar{u}ho$ = mean wind speed at 10 m height.

- **Bild 2**
  Untere Randbedingungen im Fall I nach PRUEMM (1976). $\bar{s}_0$ = trockenstatische Energie an der Meeresoberfläche, $lu|_{10}$ - Betrag der Windgeschwindigkeit in 10 m Höhe.

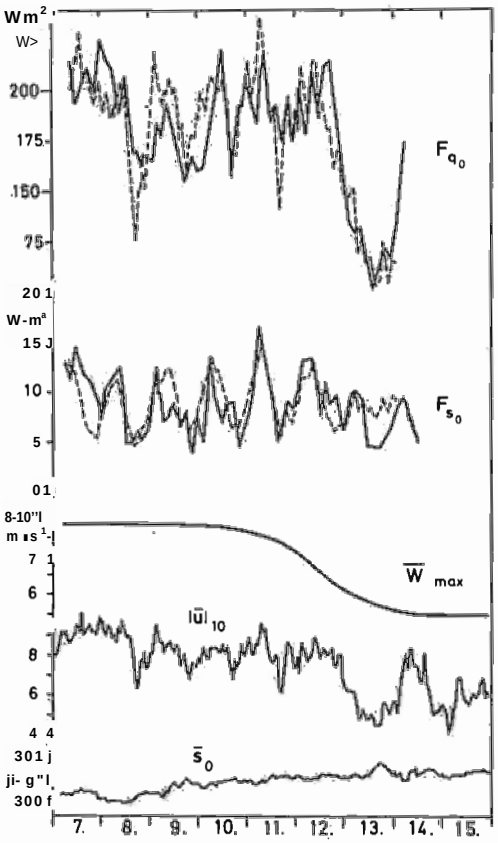

- **Figure 3**
  Lower boundary conditions of case II. $\bar{s}o$ = dry static energy at the sea surface, $l\bar{u}ho$ = mean wind speed at 10 m height. $\bar{w}_{max}$ ~ mean subsidence at the level zdb ' Fq_0 ~ latent heat flux and F_{S0} = sensible heat flux at the sea surface. Full lines: ATEX measurements, dashed lines: model results.

- **Bild 3**
  Untere Randbedingungen im Fall II. $\bar{S}o$ = trockenstatische Energie an der Meeresoberfläche, $l\bar{u}ho$ = betrag der Windgeschwindigkeit in 10 m Höhe. $\bar{w}_{max}$ = mittlere Absinkbedungung im Niveau Alb ' Fq_0 ~ latenter Wärmefluß und F_{S0} « sensibler Wärmefluß an der Meeresoberfläche. Ausgewogen: ATEX-Messungen, gestrichelt: Modellergebnisse.

time steps. At the upper boundary z_t, a constant specific humidity is prescribed, and the dry static energy fluctuates around a constant value. This oscillation is due to the diurnal solar heating prescribed by Equation (29). Besides demonstrating results with the above quoted upper boundary conditions, we will subsequently show the effect of certain linear trends of these values on the model development, as well.

3 Model Adjustment, Sensitivity Tests

On the basis of the aforementioned simplifications and hypotheses, k and 3 are the two System Parameters available for model tuning. In the two cases considered by this paper, the lateral exchange coefficient averaged over the active cloud layer 8 is calculated with the aid of Equation (25), using Constants $a = 1.28 \cdot 10^{-3}$ and $ß = 7.6 \cdot 10^{1}$. But tests with modified lateral exchange conditions will also be carried out. A proper fit between the initial model conditions and the observed surface fluxes is obtained for the turbulent transfer coefflcients $c_h = 1.35 \cdot 10^{-3}$ and $c_e = 1.45 \cdot 10^{-3}$. These values fall into a rather central position in the scatter regime of empirically determined values for the trade wind area (see e.g. POND et al., 1971; DUNCKEL et al., 1974; KRUEGERMEYER,1975), and are applied to our Simulation computations.

In both of our cases, a satisfactory Simulation of the observed boundary layer structure is achieved for k = 0.24, which is in good agreement with results obtained for pure mixed layer models. According to DEARDORFF(1976), these center on 0.25. Sensitivity tests with case I data are compiled in Table 2. The structure of the ABL is represented by the heights of the mixed layer (z_m) and the cloud layer (zjt) after 1,3, and 5 days of Simulation, as well as by the mean double amplitude (A) of the diurnal height change of these boundaries (see the right hand side of Table 2). The convective activity is indicated by the minimum and maximum value of the mean diurnal wave of $\bar{w}j$. The results of each of the various test runs with modified parameters, in Table 2, should be compared to the data of the first line. These refer to "normal" conditions, which provide a good fit between observations and computations.

■ Table 2 Changes of the height of the mixed layer z_m, the top of the cloud layer zjt and the cloud motion w*, due to variations of the system parameter k and the layer averaged lateral exchange parameter 6*. Columns 1., 3., 5. and A indicate day of Simulation and mean diurnal double amplitude, respectively. For w* the mean daily minima (min) and maxima (max) are indicated. Units are marked in brackets.

■ Tabelle 2 Änderungen der Höhe der durchmischten Schicht z_m, der Wolkenobergrenze zjj und der Wolkenbewegung w* infolge unterschiedlicher Werte für den Systemparameter k und den vertikal integrierten lateralen Austausch $\tilde{S}$*. Die mit 1., 2., 3. und A bezeichneten Säulen markieren den Simulationstag bzw. die mittlere Doppelamplitude des Tagesganges. Für Wg sind die mittleren täglichen Minima (min) und Maxima (max) eingetragen. Die Einheiten sind in Klammern angegeben.

modification	line	model parameters k	«»(lO-Sm"¹)	z_m (m) 1.	3.	5.	A	ABL quantities $\bar{Z}$dt(m) 1.	3.	5,	A	w£(10 ² ms •) min	max
"normal" case	1	0.25	1.75	590	590	590	60	1650	1650	1650	100	1.9	4.2
k: - 28%	2	0.18	1.75	560	540	540	50	1550	1500	1500	100	1.6	3.6
k: + 40%	3	0.35	1.75	650	640	635	60	1700	1950	2350	75	2.5	4.3
$\tilde{6}$*: + 20%	4	0.25	HP	590	580	580	50	1500	1500	1500	100	2.8	5.2
6*: - 20%	5	0.25	1.40	600	585	585	50	1700	1750	1800	100	1.5	3.5

Mödifications of the System parameter k and the vertically integrated lateral eschtmge function qualitatiwly influence the model behaviour in an understandable way. Reactions to variations of $\tilde{8}^*$ are more or less restricted to the cloud layer. It is interesting to note that the increase and decrease of lateral mass exchange, due to variations of $\tilde{8}^*$, are amplified by simultaneous alterations of the cloud motion w*. Differences of k are reflected in both the mixed and cloud layer heights with stronger deflections of the latter. In general, these numerical experiments demonstrate that uncertainties of k and $\tilde{8}^*$, which are less than ± 20 %, only have a minor influence on the model ABL for prognostic periods of less than 3 days, and they have practically no effect on the diurnal oscillation.

4 Results

4.1 Mean Diurnal Changes of the ABL (Case I)

The Simulation of the mean diurnal changes of the boundary layer structure has been carried out for 5 consecutive cycles. The build-up time of the model, after which the diurnal period is established, seems to be somewhat less than one day. One might recognize this from the time height cross-section of s and q in Figure 4. The diurnal variations of both of these quantities in the various layers are clearly depicted from the second day and on. The passive cloud region is marked by the steep gradients in both, the dry static energy and specific humidity. The diurnal waves of specific humidity and to a less degree, of dry static energy of the active cloud layer show distinct phase differences to those of the layers above and below. These features will be subsequently explained as consequences of cumulus convection.

The following model results represent time averages of Simulation days 2 through 5, in order to eliminate high frequency numerical noise and build-up effects in the model. The diurnal Variation of cumulus

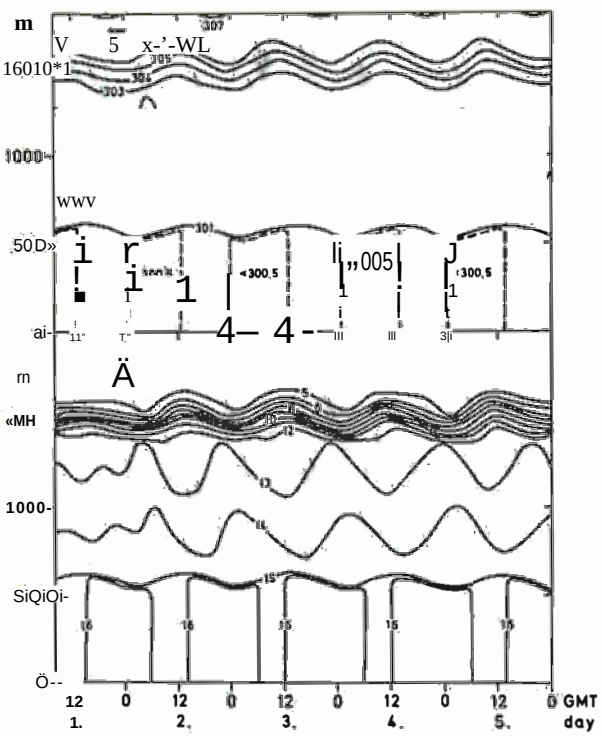

- **Figure 4**
  Time height cross-section of dry static energy s (J g^{-1}) and specific humidity q (g kg^{-1}) for 5 days of Simulation under case I conditions.

- **Bild 4**
  Zeithöhenschnitt der trockenstatischen Energie s (J g^{-1}) und spezifischen Feuchte q (g kg^{-1}) für 5 Simulationstage unter Bedingungen des Falles I.

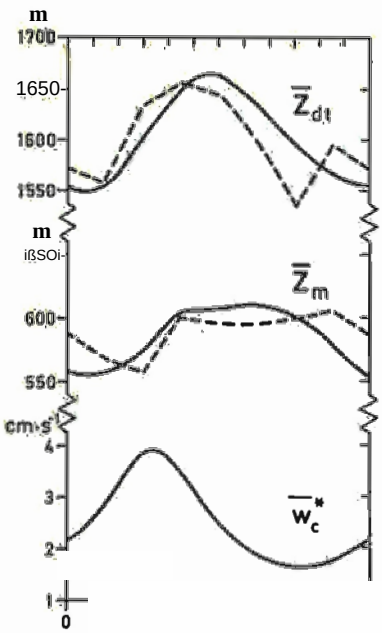

- **Figure 5**
  Mean diurnal Variation of vertical cloud motion wj, height of the mixed layer z_m and top of the cloud layer z_t. Full lines: model results, dashed lines: ATEX observations.

s **Bild 5**
Mittlerer Tagesgang der vertikalen Wolkenbewegung w*, der Obergrenze der durchmischten Schicht z_m und der Wolkenobergrenze $\bar{z}$. Ausgezogen: Modellwerte, gestrichelt: ATEX-Messungen.

convection and its impact on the mixed and cloud layer heights are depicted in Figure 5. The computed behaviour of the layer boundaries (full lines) is in satisfactory agreement with the ATEX observations (dahed lines). Shortly before sunrise, when the convective activity reaches its maximum, both the cloud layer and the mixed layer grow upwards. Their vertical extension shrinks during the aftemoon in reasonable correlation to reduced cumulus convection. The broadened peak of z_m is obvious from observations and in the model curve. According to Equation (9), in the latter case it is caused by the temperature and moisture content of the gradient layer air. During the moming hours, the water vapour of the entire subcloud layer is diminished by the drying effect of enhanced convective' upward transports at the top of the mixed layer. This process overbalances the influence of the radiatively lowered temperature on the LCL, and causes the upward motion of z_m. During the aftemoon, the radiative warming's influence on the LCL is, by and large, compensated for by the simultaneously growing moisture content, so that the model mixed layer depth remains constant. Around midnight, the specific humidity near the sea surface atteins its maximum due to the reduced convective activity in the previous hours and the air temperature is decreasing after sunset. Thus, both of these quantities act on the LCL in the same direction and thereby force z_m and the cloud base downwards. The curve of the cloud motion is in qualitative agreement with the hourly observations of low level clouds during ATEX, which show a maximum cloud coverage at about 09.00 GMT and a minimum at 00.00 GMT.

The vertical divergence of convective and small scale turbulent transports of thermal energy and water mass, which actually influence the mean quantities of i and q, can be visually derived from the fluxes of Figures 6 and 7. The solid lines represent model results, and the dashed curves are deduced from ATEX budget studies. Both the observed and computed fluxes roughly agree at the 10 m level. A qualitatively similar time Variation of the ATEX and model transports may still be found at the top of the mixed layer z_m, as well as at the cloud layer level z , for the upward flow of water mass $F_{q+ß}$. Such a correlation can no longer be seen between the observationally and numerically determined energy fluxes F_s and F;* at the same boundaries. This negative result is not surprising, since the observational determination of small scale fluxes of dry static energy, as a residual of large scale budgets, suffers from a consider-

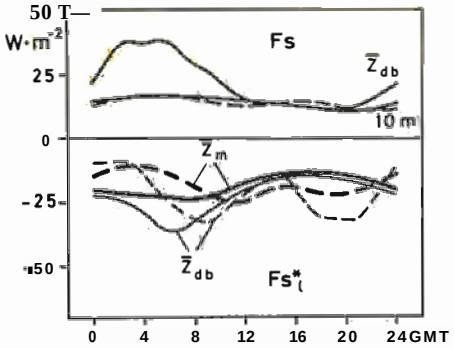

- **Figure 6**

  Vertical fluxes (positive: upwards, negative: downwards) of dry static energy (Fs) at 10 m height, at the base (z_m) and at the top ($\bar{z}jb$) of the active cloud layer. Fsß = energy flux at $\bar{z}jb$ including the effect of condensation and evaporation (see text for explanation). Full lines: model results, dashed lines: ATEX observations.

- **Bild 6**

  Vertikale Flüsse (positiv: aufwärts, negativ: abwärts) trockenstatischer Energie (Fs) in 10 m Höhe, an der Basis (z_m) und an der Obergrenze (z_d b) der aktiven Wolkenschicht. Fsß = Energiefluß unter Berücksichtigung der Verdunstungs- und Kondensationseinflüsse (siehe Text für weitere Erklärung). Ausgezogen: Modellergebnisse, gestrichelt: ATEX-Werte.

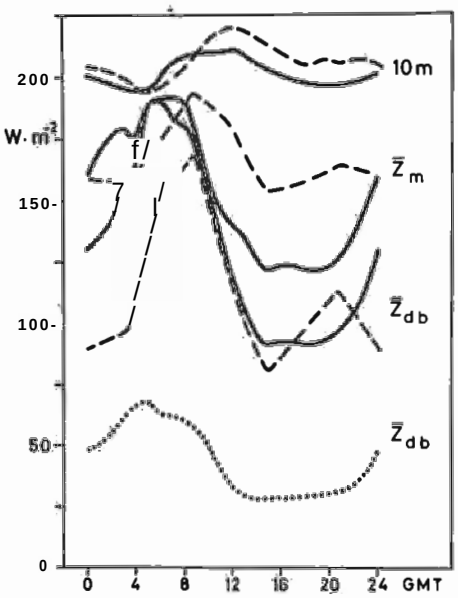

- **Figure 7**

  Vertical fluxes of latent heat of water vapour (F_q) at 10 m heigt and cloud base z_m and of latent heat of water vapour and liquid water (F_q + ß) at $\bar{z}_d$ b derived from model calculations (full lines) and from ATEX-observations (dashed lines). Dotted curve: Flux of latent heat of liquid water (Fß) at $\bar{z}_d$ b-

® **Bild 7**

  Vertikale Flüsse der latenten Wärme des Wasserdampfes (F_q) in 10 m Höhe und an der Wolkenbasis $\bar{z}_m$ sowie der latenten Wärme des Wasserdampfes und des flüssigen Wassers (F_q + ß) im Niveau $\bar{z}_d$ b nach Modellrechnungen (ausgezogen) und nach ATEX-Messungen (gestrichelt). Punktiert: Fluß latenter Wärme des Flüssigwassers (Fß) in der Höhe zjb ■

ably higher degree of uncertainty than do the similarly derived subgrid scale water mass transports. The first ones are about two Orders of magnitude smaller than the respective mean flow values, while the latter ones are equivalent to the respective large scale transports.

According to the curves in Figure *6*, the subcloud layer is heated by the turbulent and convective fluxes throughout day and night, since F_s is continuously directed upwards at 10 m height and downwards at z_m. About 45 % of this thermal energy input is advected away downstream by the large scale flow, and the other approximately 55 % is required for balancing the radiative cooling of the mixed layer.

For the cloud layer, where according to our assumptions we have $F_s = F_s{}^*$ at the level z_m and $F_s = F_s{}^* = 0$ at the top of the passive cloud layer z_{dt} the model results of Figure 6 indicate: a) The passive cloud layer is permanently cooled by evaporation of cloud droplets, which accounts for the difference between F_s and $F_s{}^*$ at the level z_d b- This cooling, which is largest around 06 GMT and

smallest at 16 GMT, roughly varies in phase with the diurnal radiative cooling. b) The active cloud layer is slightly warmed by convection from about 02 GMT to 10 GMT, i.e. (Fsg_{Zm} - $Fs\dot{s}_{Z(Jb)}$) > 0, while the cloud process does not affect the heat budget of this regime during the rest of the day. Consequently, here, the convectively and radiationally created diurnal temperature changes are about 180 degrees out of phase. The condensational warming during the night diminishes the purely radiatively induced temperature wave in the active cloud layer, and displaces its minimum from 08 GMT to about 04 GMT, as already mentioned in connection to Figure 4.

The latent heat transports at z_m and Zd_b in Figure 7 are strongly correlated with the vertical cloud motion in Figure 5. It is particularly interesting to note that during the time of most intense convection, around 06 GMT, nearly the entire water mass (for the share of liquid water see lower dotted curve), which evaporates at the sea surface, is transported into the passive cloud layer. Consequently, cooling as well as moistening of the upper cloud region in the trades has its maximum during the hours before sunrise. In contrast, the moisture content of the mixed layer and the active cloud layer is increased during the afternoon interval of depressed cumulus convection. This is when about 50 % of the water vapour input from the sea surface is deposited below zj_b. This behaviour of the latent heat or water mass transports leads to the previously mentioned phase shifts of the diurnal oscillations of specific humidity, which measure nearly 180 degrees across the top of the active cloud layer Zd_b •

In this connection, we would like to further point out that the diurnal cycle of cumulus convection also causes significant modifications of the sea surface evaporation (indicated by the upper curve in Figure 7). The increased water vapour fluxes between 06 and 16 GMT, which appear in the observations and in the numerical Simulation, are solely caused by variations of the convective latent heat transports. In a more detailed discussion, AUGSTEIN (1980) shows that this hump completely vanishes in the model result when the cloud motion wj is prescribed as time independent by its daily mean value. By introducing constant sea surface fluxes of sensible and latent heat in a specific test run, we will later demonstrate that both of these transports have no significant impact on the diurnal oscillation of cloud convection, and of the layer height variations mentioned earlier.

Therefore, these latter phenomena would most likely originate in the model from one or both of the two prescribed processes with inherent diurnal modes, namely the large scale subsidence and the radiatively induced air temperature changes. Considering the diurnal Variation of large scale subsidence first, we find its influence on convection and the ABL structure to be negligibly small. However, radiation appears to be an important control of the model boundary layer development, as can be concluded from Table 3. This list compiles the influence of several quantities of the large scale field and of radiation (specified on the left hand side) on the height of the mixed layer (z_m), the top of the cloud layer (z t) and the cloud motion (w*) (indicated on the right hand side of the same table). Line 1 of Table 3 represents the "normal" case, which is well adjusted to the observations, for comparison. The altered input quantities on the left hand side are underlined. The results of the following test computations are in reality only meaningfull in a qualitative way, since we do not know to what extent our model concept would still be valid under the artificially introduced large scale conditions.

Reactions of the model ABL to certain possible changes in the radiatively generated diurnal temperature wave are documented by lines 2 through 5 of Table 3. Of particular interest is the case without any temporal variations of radiative heating (i.e. c = d = e_c = 0 in line 2). Then, the diurnal oscillation of the layer boundaries and of $\bar{w}j$ practically vanishes, and the top of the cloud layer continuously migrates upwards during the first 5 days of Simulation. The increase in the amplitude of the height independent temperature change (c = 0.6 $K\,d^{-1}$, line 3) as well as the growth of its amplitude with height (d = 1.5 ▮lO $K\,d^{-1}\,m^{-1}$, line 4) cause the following effects: the vertical deflection of the 24-hourly oscillations of the layer boundaries is increased, the mean vertical extension of the cloud layer is dimnished, and the amplitude of the fluctuations of w_c^* is enhanced.

Table 3 The effect of radiation, mean subsidence, horizontal advection and boundary confiöäns on the ABL structure and vertical cloud motion w£. The raÄiion Parameters c, d and e_c refer to equation (29) in text. w_{max} = subsidence at top of active doudi fevel zjb. q_{acjv} and $s_a d_v$ indicate horizontal advection. Line 10 stetes the effects of linear change in time of the upper boundary conditions $q_z t$ and Szt. Line 11 shows results with time independent surface fluxes. For explanation of the right hand side of this table see legend of Table 2.

Tabelle 3_Dar Einfluß der-Strahlungj desjnittferen, Absiitkens, der horizontalen Aclvsklion und der Rajid.bedifligttngen.'attf dle-Greiizscdiichtstrukturiiud-die Wölkenbö-wegung w_c . Die Strahlungspuameter c, d und 6 beziehen sieh auf die .Gleichung (2.-9) des Textes. w_{ra3} k ~ Absinkbewegung an der Übergr&nze der aktiven Wolken-schicht zdb- Qadv und Sadv bezeichnen die horizontale Advektion. Zeile 10 steift die'Wirktmg.einer zeitlich linearen Änderung der oberen Randbedingung $q_z t$ und T_{zt} dar. In der Zeile 11 sind die Flüsse an der Meeresoberfläche zeitlich konstant gehalten. Die rechte Seite dieser Tabelle entspricht den Angaben zu Tabelle 2.

modified quantities	line	radiation: c (Kd-i)	radiation: d	radiation: ®c (Km -1)	mean flow: $\bar{w}_m$ (10^{-3} s^{-1})	mean flow: Qadv	mean flow: Apa$_s$	ABL quantities: $\bar{z}_m$ (m)				$\bar{z}_{dt}$ (m)					
								[illegible]	[illegible]	[illegible]	A	[illegible]	[illegible]	[illegible]	A	[illegible]	[illegible]
[illegible]	1	[illegible]	0	0	[illegible]	[illegible]	- 2.[illegible]	[illegible]	[illegible]	[illegible]	60	1650	1650	1650	[illegible]	[illegible]	4.[illegible]
radiation	2	[illegible]	0	0	[illegible]	[illegible]	[illegible]	[illegible]	[illegible]	[illegible]	[illegible]	[illegible]	[illegible]	[illegible]	[illegible]	[illegible]	3.0
	3	[illegible]	0	[illegible]	[illegible]	[illegible]	[illegible]	[illegible]	[illegible]	[illegible]	[illegible]	[illegible]	[illegible]	[illegible]	[illegible]	[illegible]	5.0
	4	[illegible]	$1.5 \cdot 10^{-4}$	[illegible]	[illegible]	[illegible]	[illegible]	[illegible]	[illegible]	[illegible]	[illegible]	[illegible]	[illegible]	[illegible]	[illegible]	[illegible]	5.0
	5	[illegible]	0	[illegible]	[illegible]	[illegible]	[illegible]	[illegible]	[illegible]	[illegible]	[illegible]	[illegible]	[illegible]	[illegible]	[illegible]	[illegible]	4.0
mean subsidence	6	0.4	0	0	- 8.2	[illegible]	[illegible]	[illegible]	580	X	[illegible]	1350	1100	X	[illegible]	[illegible]	7.[illegible]
	7	0.4	0	[illegible]	- 5.0	[illegible]	[illegible]	[illegible]	600	X	[illegible]	1800	2400	X	[illegible]	[illegible]	4.[illegible]
horizontal advection	8	0.4	[illegible]	[illegible]	[illegible]	[illegible]	[illegible]	710	680	X	[illegible]	1850	[illegible]	X	[illegible]	[illegible]	4.[illegible]
	9	0.4	[illegible]	0	[illegible]	[illegible]	[illegible]	570	580	575	[illegible]	1550	[illegible]	1490	[illegible]	[illegible]	4.[illegible]
[illegible]	10	0.4	[illegible]	[illegible]	- 6.[illegible]	[illegible]	[illegible]	[illegible]	[illegible]	[illegible]	50	1625	[illegible]	1400	[illegible]	[illegible]	4.[illegible]
(w's')o = const (w'q')o = const	11	0.4	0	[illegible]	[illegible]	[illegible]	[illegible]	[illegible]	[illegible]	[illegible]	50	1600	1650	1650	10[illegible]	1.7	4.[illegible]

An increase of the diurnal temperature wave in the cloud top region is manipulated by setting $e_c = 0.5\ K d^{-1}$ in the passive cloud layer, and zero everywhere eise (line 5). This alteration leads to an amplification of the vertical displacement of the layer boundaries z_m and za_b. The amplitude, primarily of the oscillation of z_m, grows with increasing values of e_c and our model already collapses for $e_c = 1.0\ K d^{-1}$ after a short period of model time. According to these results cloud top cooling and its time variations may induce considerable modifications of the ABL structure, if cloud tops are concentrated on a relatively thin layer like in presence of stratocumulus. In our observational case, the trade-wind cumuli form an ensemble with cloud tops spread out over a rather deep region. Therefore, it is not too surprising that obviously in nature radiative cooling of the cloud surfaces does not significantly couple back on the convection process.

From the previous numerical experiments, we conclude that diurnal temperature variations with a height independent amplitude of 0.4 K, caused by radiation, may initiate the observed diurnal changes of the ABL structure and of cumulus convection in the undisturbed tradewind zone.

An analysis of the various quantities of Equation (13) reveals that modifications of the cloud motion w‘ predominantly result from the temperature difference ($\overline{\theta}_{v1O}$ - $\overline{\theta}_{vzb}$)- Since the diurnal Variation of the temperature in the “normal” case (induced by Equation (29)) is constant with height, it does not directly modify the quoted temperature difference. The indirect influence of radiation on this quantity through the surface heat and water vapour fluxes is also insignificant, as can be seen from the experiment indicated on line 11 of Table 3. From a detailed investigation of the development of the model ABL, we find the following chain of events: The radiatively created temperature change primarily modifies the condensation rate of water vapour via its influence on the water vapour Saturation value of air. This immediately leads to variations of the condensational heating of the active cloud layer, and by that causes changes in the virtual temperature at cloud base 0 and finally, of ($\overline{\theta}_{v1O}$ - $\overline{\theta}_{vzb}$). This chain of processes becomes obvious through the model computations and has, in its general meaning, already been considered by KRAUS(1963) to explain the diurnal height variations of the boundary layer depth at Weather Ship N in the Pacific Ocean. In contrast to our Situation, KRAUS(1963) assumed that the cloud layer was occupied by stratocumulus clouds.

The influences of the mean large scale vertical motion and horizontal advection on the boundary layer development are shown by the results on lines 6 to 9 of Table 3. The’importance of both of these processes on the long term behaviour of the ABL becomes clearly obvious. Model days, in which the cloud layer has exceeded the upper boundary of the model or has shrunk below 200 m in depth are marked by crosses in Table 3. The large value of $7 \cdot 10^{-2}\ m\ s^{-1}$ for w£ on line 6 does not seem to be realistic. We speculate that in nature, the strong subsidence would force cumulus clouds to vanish rapidly and consequently, our model would fail to describe the ABL characteristics.

Reduced (line 8) or enhanced (line 9) horizontal advection of cold and dry air causes both the mixed layer and the cloud layer to grow or to shrink, respectively. Since horizontal advection is restricted to the mixed layer in our case, similar effects could be induced on the ABL development through modifications of the sea surface temperature, which would alter the sensible heat and water vapour input from below. Changes in the upper boundary conditions (e.g. a temporal increase of s_{zt} and q_{zt}, as indicated on line 10) also have a distinct influence on the-vertical structure of the boundary layer. In this particular case, the advective heating at the upper boundary of the model increases the static stability of the free atmosphere and thus, hinders the upward cloud growth. The temporal moisture increase at the top finally spreads across the entire ABL and thus, also migrates down to the surface layer. The consequence of this being that the LCL of the air at 10 m and concurrently the height of the mixed layer are lowered.

4.2 The ATEX Time Period From 7.2. to 14.2.1969 (Case II)

During the entire case II time period, two of the comer ships of the ATEX triangle maintained their positions in a steady horizontally divergent tradewind flow. However, the most southerly ship, the "METEOR", got in touch with the fringes of the ITCZ from the 12th to the 14th of February. Therefore, the large scale conditions were less uniform at the end of the experimental phase than at the beginning.

The initial, boundary and large scale conditions of the model calculations are partially listed in Table 1 and partially graphed in Figure 3. The coefficients $\ddot{a}, \hat{b}, \hat{d}$ and e_c of the radiation formula (Equation (29)) in case II are the same as in the "normal" version of case I. With the so chosen large scale values and radiation conditions, the long term behaviour, namely the slight growing with time of the dry static energy and specific humidity in the subcloud and cloud layers during ATEX is roughly approximated by the model results, as shown in Figure 8. The daily mean values of the top of the ABL zj_t and the height of the mixed layer z_m are plotted on Figure 9. The gross features of the measured long term changes of both layer boundaries are reproduced by the calculations, but distinct discrepancies are found in several details.

A rather obvious difference is the model's systematic underestimation of zj_t during the first 4 days and its overestimation during the last 3 days of the case II time period. These facts result from the model assumptions that the horizontal advection of dry static energy within the passive cloud layer is constant and the small scale heat flux from the passive cloud layer into the free atmosphere is taken as zero. According to WAGNER's (1975) analysis, this flux is particularly large before the 10 th of February and becomes zero or even changes sign during the rest of the time. Therefore, the prescribed advective cooling of the model's passive cloud layer is too small at the beginning of the phase and too large at the end, when compared to reality.

The calculated mixed layer height z_m in Figure 9 is constantly lower than the observed one during the last 4 days of the period. This offset could be reduced by a slightly larger horizontal advection of dry air starting on the lOth of February. Both of the above mentioned differences between model results and measurements again demonstrate the high sensitivity of the ABL to the large scale flow parameters. This may realistically reflect the natural process, since it would help to explain the strong variations in the height of the tradewind inversion, as observed by AUGSTEIN et al. (1974) over the Atlantic Ocean.

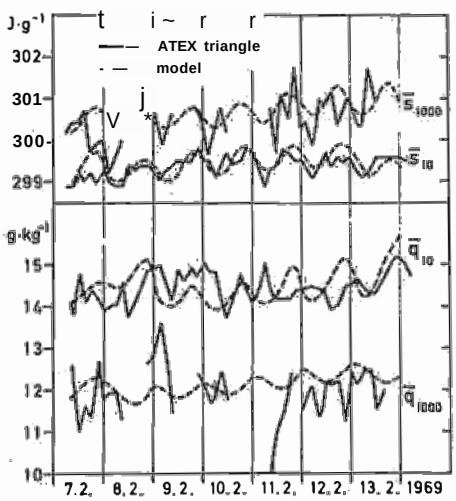

- Figure 8
  Time series of dry static energy $\bar{s}$ and specific humidity $\bar{q}$ at 10 m and 1000 m height.

- Bild 8
  Zeitreihen der trockenstatischen Energie $\bar{s}$ und der spezi-* fischen Feuchte $\bar{q}$ in 10 m und 1000 m Höhe.

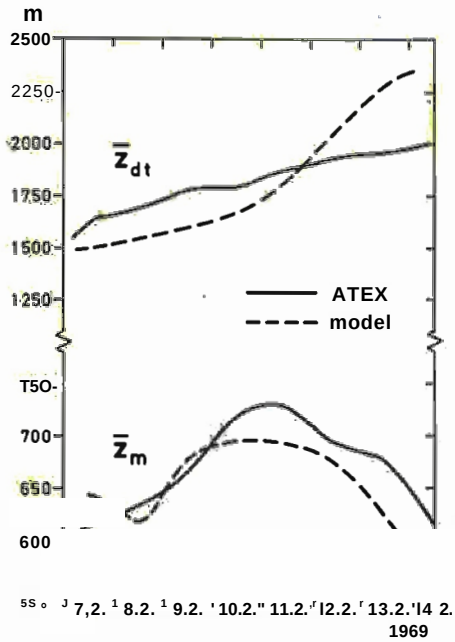

® Figure 9

The top of the atmospheric boundary layer $\bar{z}jj$ and of the mixed layer $\bar{z}_m$ during the first period of ATEX. Triangulär daily mean from measurements: full lines. Model: dashed lines.

• Bild 9

Der obere Rand der Grenzschicht $\bar{z}j_t$ und der durchmischten Schicht $\bar{z}_m$ für die erste ATEX-Periode. Tagesmittelwerte für das Dreieck aus Messungen: ausgezogen. Modellwerte: gestrichelt.

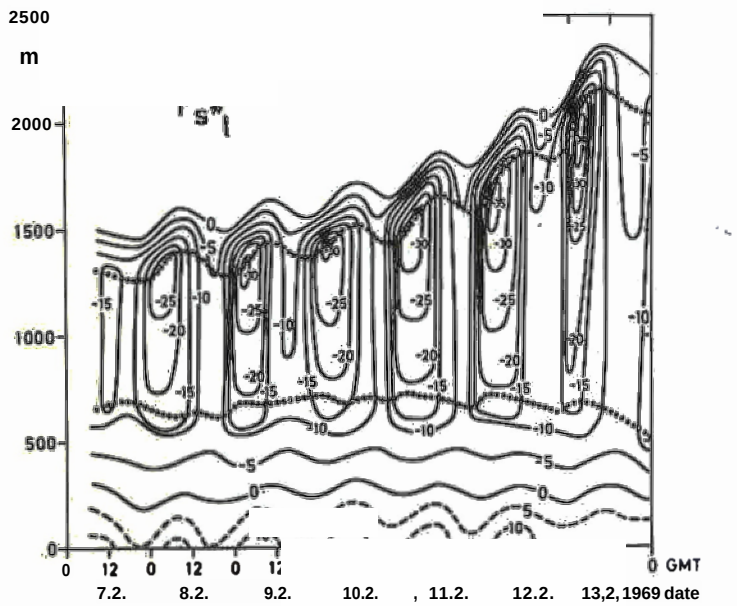

® Fjgure 10

Time height cross-section of vertical flux of thermal energy including the effect of condensation and evaporation. Numbers indicate transports in $W m^{-2}$. Full lines: downward fluxes, broken lines: upward fluxes. Dotted curves mark levels of $\bar{z}db$ (upper line) and of $\bar{z}_m$ (lower line).

• Bild 10

Zeithöhenschnitt des Vertikaltransports thermischer Energie unter Berücksichtigung von Kondensation und Verdunstung. Zahlenwerte in Wm^{-2}. Ausgezogen: abwärtsgerichtete Flüsse, gestrichelt: aufwärts gerichtete Flüsse. Punktierte Kurven bezeichnen die Niveaus von $\bar{z}jf$ (oben) und $\bar{z}_m$ (unten).

Some further features of the numerical investigation of the ATEX time series are displayed by the isolines of the vertical fluxes F_s* in Figure 10, and $F_{q+ß}$ in Figure 11. The values between the layer boundaries have been obtained by a linear interpolation. This is a reasonable approximation of the actual pattern according to computations with the grid point Version of the model. Diurnal variations of these basically cloud related transports and their effects on the upper lid of the cloud layer are clearly depicted. Between

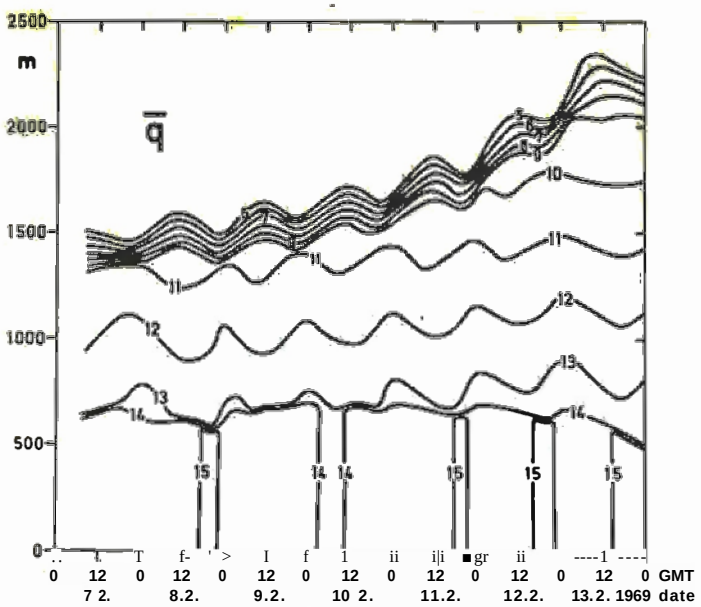

Figure 11

Time height cross-section of specific humidity of case II from model calculations.

- **Bild 11**

Zeithöhenschnitt der spezifischen Feuchte für den Fall II aus Modellrechnungen.

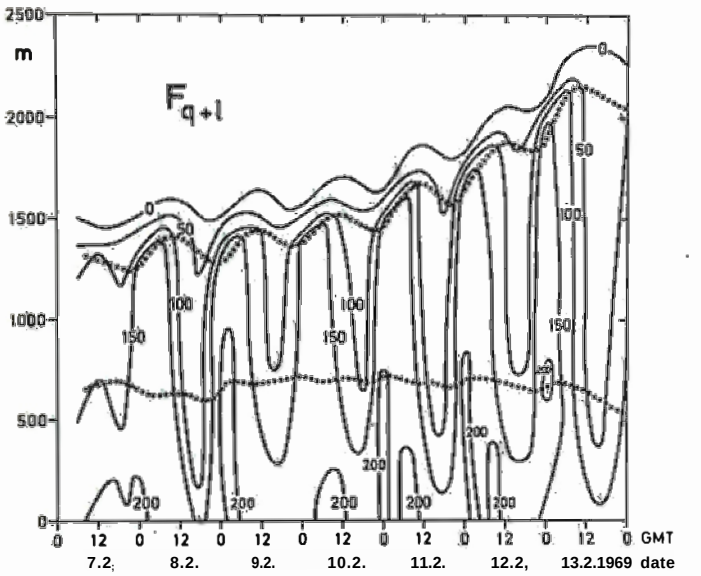

- **Figure 12**

Time height cross-section of vertical flux of latent heat of water vapour and liquid water in $W m^{-2}$ (for dotted lines see Figure 10).

- **Bild 12**

Zeithöhenschnitt des Vertikaltransportes latenter Wärme des Wasserdampfes und des flüssigen Wassers in $W m^{-2}$ (punktierte Linien: siehe Bild 10).

0 and 12 GMT during the first half of the day, the passive cloud layer suffers a considerable cooling due to the high values of downward directed F_s* at z b (upper dotted curve on Figure 10). This vertical flux divergence decreases the static stability of the layer, and favours cloud growth into the free atmosphere. In spite of the thereby entrained dry air from above, the water vapour content of the passive cloud layer (Figure 11) stays nearly constant in time. This is due to the fact that the upward water mass transport Fq +2 (Figure 12) is also increased during the same time interval.

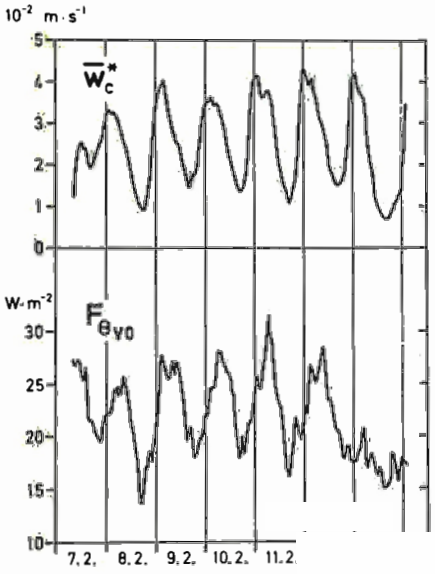

® Figure 13
Vertical cloud velocity (w*) and buoyancy flux at sea surface (F_{0yO}) derived from model computations.

• Bild 13
Vertikale Wolkenbewegung (wj) und Auftriebstiansport an der Meeresoberfläche (Fq_{vQ}) nach Modellrechnungen.

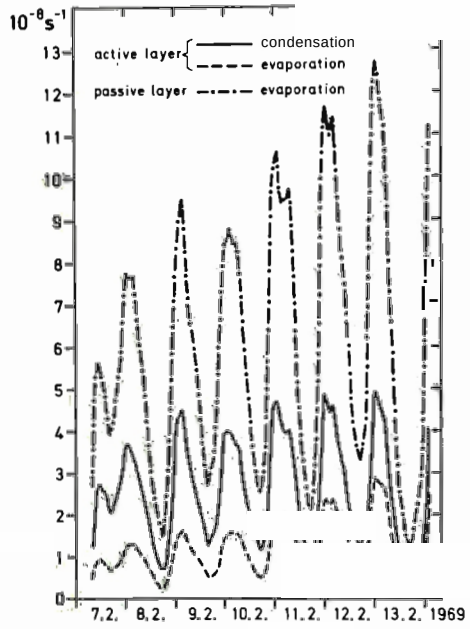

® Figure 14
Condensation rate and evaporation per unit air mass in the active and passive cloud layers.

• Bild 14
Kondensationsrate und Verdunstung pro Luftmasseneinheit in der aktiven und passiven Wolkenschicht.

The vertical cloud motion w* (Figure 13) is fairly constant in its long term behaviour, but is again governed by a strong diurnal component. The phase relationship between the 24-hourly mode of *w** and the surface buoyancy flux $F_{0y()}$ (lower curve in Figure 13) confirms the earlier conclusion that F_{0yO} does not trigger the diurnal mode of the vertical cloud motion, but that the opposite is more likely under trade wind conditions over the ocean. Over land surfaces the Situation should be quite different since the diurnal variations of surface heat fluxes are an Order of magnitude larger than over water.

Düring the night, when solar heating is zero, the process cycle reverses its sign so that the top of the could layer migrates upward again. Obviously, the diurnally changing convection has an asymmetric impact on the cloud layer height, due to the nonlinear dependence of the Saturation specific humidity on temperature. Neglection of the diurnal mode of solar heating in the model experiment yields a rapid upward displacement of the top of the cloud layer in contrast to observations.

Satisfactory agreement between the observed and computed mixed layer depths is achieved for the mean diurnal changes (case I), as well as for the 7-day time period (case II). The similarity between measurements and computations (e.g. the determination of the model mixed layer height z_m by the lifting condensation level of air at 10 m height) Supports the hypothesis that z_m mainly depends on the thermodynamic state of the subcloud layer air.

6 Acknowledgements

We wish to thank Prof. H. KRAUS and an unknown referee for their detailed reviews of this article which led to considerable improvements of the text.

We are deeply indebted to Prof. H. RIEHL who extensively supported our investigations in the low latitudes. In particular one of the authors (E.A.) has benefltted from his expertise of the tropical atmosphere during several cooperative efforts.

Appendix

The Model Equations

The full set of model equations is obtained by Integration of Equations (1) and (2) with respect to the height z to form layer averages for the layer below z_m, the active cloud layer, the passive cloud layer and the free atmosphere. We assume that within each layer the mean values of s, q and the cloud properties 's*, q* and change linearly with height. Making further use of Equations (3), (4), (7), (8), (9), (10), (11), (12), (13), (14), (15), (18), (19), (20), (21), (22), (25), (26), (28) and (29) one achieves a closed set of equations for the ABL. These are noted subsequently with the unknown quantities on the left hand side. The layer averages of dry static energy and specific humidity s and q, respectively, are determined prognostically and all the other properties result from diagnostic equations. Starting from the lower boundary we have the following relationships:

a) Sea Surface

$$F_{so} = P(\overline{w'0'})_o = c_H\ p(s_0 - s_{io})\ 1^u\ 110 \qquad \text{(A1)}$$

$$F_{qo} = pL(\overline{w'q'})o = c_E\ Lp(q_{s0} - qio)\ lulio \qquad \text{(A2)}$$

$$F_{\text{©}Vo} = P(w'\ddot{O}Oo = F_s o + \frac{0.608\ Sio}{L}\ F_{q0} \qquad \text{(A3)}$$

$$S10 = \frac{\tilde{s}_m + 0.184\ s_0}{1.184} \qquad \text{(A4)}$$

$$q_{\text{‹o“}} = \frac{\tilde{Q}m"t0.161\ q_s o}{1.161} \qquad \text{(A5)}$$

b) **Mixed Layer**

$$\frac{d}{\partial t} \tilde{®m} = \frac{1}{...} \left[7 \frac{d^z m}{Jt} + \overline{}_{zm} / (\bar{s}_m - \bar{s}_{zb}) \quad \overline{W}^*_c (s_c^* \sim s)_{zb} + \frac{Fso}{\sim \rho} - \frac{1}{\sim \rho}(\overline{R}_{zm} \quad \overline{R}_0) + \tilde{S}adv \right] \qquad (A6)$$

$$\frac{3}{\partial t} \tilde{Q}m \text{“} £\frac{1}{m} \left[\left(- \frac{dz_m}{dt} \text{-b} \, \overline{w} \, zm \right) (Qm \sim Qzb) - \overline{w} \, c \, (Qc \text{“} \, Q)zb + \frac{F_{*Qo}}{-r} + \frac{1}{} Qadvj \right] \qquad (A7)$$

$$Zm = LCL_{(710} \quad q_{10} \quad p_{(z))} \qquad (A8)$$

c) **Active Cloud Layer**

$$\frac{3}{\partial t} \tilde{S} - (zjb \frac{1}{-z} \quad J \quad \overline{w} \, zdb \, C \, zdb - \tilde{s}) + W_{zm} \, (s_{zm} \sim \tilde{s}) + W_c \quad fSfic \sim {}^s)zdb + ({}^s ßc \sim \text{'}Ozm \}$$

$$- \frac{1}{p}(Rzdb - Rzm) \text{"*■} \frac{dz_{db}}{ut} \quad (\$zdb \text{””} {}^s) - \frac{dz_m}{dt} ({}^s zm - {}^s)] \qquad (A9)$$

$$\frac{9\tilde{q}}{Öt} = \frac{1}{(z_{db} - z_m j} \quad Wzdb \, (Qzdb \,\text{"}\, \tilde{q}) + Wzm \, (qzm \,\text{"}\, \tilde{} + W_* \{ - (\bar{q}^*_{ßc} \text{„} \, q \quad zdb + ({}^q ®^c \text{„} \, q \,)zmi$$

$$+ \frac{(1_{zdb}}{} (Qzdb■ \, q) * \frac{dZry»}{äT} (qzdb \text{ “} \frac{fY}{q)1} \qquad (A10)$$

d) **Passive Cloud Layer**

$$\frac{df}{dt} = \frac{1}{(Zd - Zdb)} \quad Wzdt <^{Szdt} , \tilde{S}) + \overline{W}zdb \quad Szdb \sim \tilde{S}) + \overline{w} \, c({}^s ßc \text{“} \, s)$$

$$- \frac{1}{\sim} (\overline{R}zdt \sim \overline{R}zdb) + \frac{dz_{db}}{dt} \quad (Szdt - \overline{{}^s}zdb)] \qquad (AH)$$

$$\frac{d\tilde{q}}{3t} \quad \frac{1}{(z_{dt} - z_{db})} [- \, w_{zdt} \, (q_z dt - \tilde{q}) + w_{zdb} \, (Qzdb - \tilde{q}) + \overline{W}c \, (qg_c - q)_{zdb}$$

$$■* \frac{dz_{db}}{d_z} \quad (Qzdt - \overline{Q}zdb)] \qquad (A12)$$

$$z_{db} \text{ results from} \begin{cases} (\bar{0}_V ßc \text{“} \, \overline{®}v)z \quad 0 \quad \text{for} \;\; z < z_{db} + 4_0 \, z \\ (\bar{0}_v \, ßc - \overline{®}v)z < 0 \quad \text{for} \;\; z > z_{db} + A_o \, z \end{cases} \qquad (A13)$$

e) **Free Atmosphere**

$$\frac{ds}{öT} = \frac{1}{(z_t \sim z_{dt})} \quad \bar{W}zt(\bar{S}zt \text{ „} \, \tilde{s}) + \overline{W}zd *<Szd* \sim \tilde{S}) \sim | \frac{1 \, z5}{Rzt} \sim \frac{d}{Rzdt} \, ' \sim \sim \frac{d^z db}{dt} \quad zdt \text{ „} \, \tilde{\bar{s}})] \qquad (A14)$$

$$\frac{d\tilde{q}}{dt} = 0 \qquad (A15)$$

f) Cloud Scheme

$$\bar{w}_c^* = -\left(\frac{d\bar{z}_m}{V\,dt} - \bar{w}_{zm}\right)\frac{(\bar{\rho}_{vm} - \bar{\rho}_{vzb})}{(\bar{\rho}_{vio} - \bar{\rho}_{vzb})} \frac{k_F \bar{\rho}_{v_0}}{\bar{p} c_p (\theta_{Vlo} - \theta_{vzb})} \tag{A16}$$

$$\overline{s's'}_{cz_m} \sim \overline{s'_{10}}, \quad \overline{e'_{cz}}_m \sim \overline{q^{*'_0}}, \quad \overline{\rho'^{cz}}_m \sim \bar{\rho} \tag{A17}$$

$$\overline{s'_c z'_{db}} = (\overline{s'_c} - \overline{s'_{EcZm}}) \frac{\tilde{\delta}}{\bar{w}_c^*} (z_{db} - z_m) (\tilde{s}_{\beta c} - \tilde{s}) \tag{A18}$$

$$\overline{Qecz'_{db}} \sim \overline{w'_c} \left(\overline{q^*_c} - \overline{q_{ecz_{jn}}}\right) - \frac{\tilde{\delta}}{\bar{w}_c^*}(z_{db} - z_m) (\tilde{G}_{\beta e} - \tilde{q}) \tag{A19}$$

$$\bar{c}^* = \begin{cases} f q_{\beta c} - q_{sc} & \text{for } q_{ec} > q_{sc} \\ 10 & \text{for } q^*_c < q_{sc} \end{cases} \tag{A20}$$

$$\tilde{\delta} = \frac{\bar{w}_c^*}{(z_{db} - \bar{z}_m)} \int_{z_m}^{z_{db}} a \exp \beta (z - 600)\, dz \tag{A21}$$

g) Auxiliary Formulae and Radiation

$$\theta = SS \frac{S}{c_P} \tag{A22}$$

$$\theta_{vE} = \theta(1 + 0.608\, q - \pounds) \tag{A23}$$

$$\theta_V = \theta(1 + 0.608\, q) \tag{A24}$$

$$\frac{\partial \bar{R}}{\partial z} = \dot{a} + \dot{b} \log z + 2\pi(\dot{c} + \dot{d} z + e_c)\cos 2\pi \frac{(t - \tau_p)}{24} \tag{A25}$$

Formula (A25) still has to be vertically integrated for the different layers. The Symbols in the Appendix have the same meaning as in the text. The tilde marks layer averages.

Horizontal advection of dry static energy and water vapour in this case is attributed only to the mixed layer but in general it might be added to the other layers as well.

The following quantities have to be prescribed: s_0, $|u|_{10}$, s_{zt}, q_{zt}, $w(z)$, s_{adv}, q_{adv} and the mean air pressure profile $p(z)$. Then the above System of equations can be solved using the routine formulae for the Saturation specific humidity and for the lifting condensation level.

References

ALBRECHT, B. A., A. K. BETTS, W. H. SCHUBERT and S. H. COX, 1979: A model of thermodynamic structure of the Trade-Wind Boundary Layer: Part I. Theoretical formulations and sensitivity tests. J. Atmos. Sei. 36, 73-89

ARAKAWA, A. and W. H. SCHUBERT, 1974: Interaction of a cumulus ensemble with the large-scale environment. Part I. J. Atmos. Sei. 31, 674—701

AUGSTEIN, E., 1976: Boundary layer observations over the oceans. Seminars on the treatment of the boundary layer in numericäl weather prediction, Reading 1976. European Centre for Medium Range Weather Forecasts

AUGSTEIN, E., 1980: Atmosphärische und ozeanische Grenzschichten in den niederen Breiten (in Vorbereitung für Hamburger Geophys. Einzelschriften)

AUGSTEIN, E., H. RIEHL, F. OSTAPOFF and V. WAGNER, 1973: Mass and energy transport in an undisturbed Atlantic trade-wind flow. Month. Weath. Rev. 101, 101-111

AUGSTEIN, E., H. SCHMIDT and F. OSTAPOFF, 1974: The veitical structure of the atmospheric planetary boundary layer in undisturbed trade winds over the Atlantic Ocean. Bound. Layer Met. 6, 129-150

AUGSTEIN, E. and V. WAGNER, 1975: Vertical coupling within the Hadley circulation over the Atlantic Ocean. Beitr. Phys. Atmosph. 48, 103-118

BALL, F. K., 1960: Control of inversion height by surface heating. Quart. J. Roy. Met. Soc. 86, 483-494

BETTS, A. **K.,** 1973: Non-precipitating cumulus convection and its parameterization. Quart. J. Roy. Met. Soc. **99,** 178-196

BRUEMMER, B., 1976; The kinematics, dynamics and kinetic energy budget of the trade wind flow over the Atlantic Ocean. "Meteor"-Forsch. Ergeb. B11, 1—24

BUNKER, A. F., B. HAURWITZ, J. S. MALKUS and H. STOMMEL, 1949: Vertical distribution of temperature and humidity over the Caribbean Sea. Pap. Phys. Ocean. Met., Mass. Inst. Techn. and Woods Hole Ocean. Inst., 83 pp

CARSON, D. J., 1973: The development of a dry inversion capped convectively unstable boundary layer. Quart. J. Roy. Met. Soc. 99, 450-467

DEARDORFF, J. W., 1976: On the entrainment rate of a strato-cumulus-topped mixed layer. Quart. J. Roy. Met. Soc. 102, 563-582

DUNCKEL, M., L. HASSE, L. KRUEGERMEYER, D. SCHRIEVER and J. WUCKNITZ, 1974: Turbulent fluxes of momentum, heat and water vapour in the atmospheric surface layer at sea during ATEX. Boundary-Layer Met. **6,** 81-106

FRAEDRICH, K., 1974: Dynamic and thermodynamic aspects of the parameterization of cumulus convection: Part II. J. Atmos. Sei. 31, 1838-1849

GRASSL, H., 1978: Strahlung in getrübten Atmosphären und in Wolken. Hamb. Geophys. Einzelschr. A37, 136 pp

HEINRICI, P., 1972: Elemente der numerischen Analysis, Band I. Bibliogr. Inst. Mannheim, S. 277

HOLLAND, J. Z. and E. M. RASMUSSON, 1973: Measurements of the atmospheric mass, energy and momentum budgets over a 500 km square of tropical ocean. Month. Weath. Rev. 101, 44-55

JOHNSON, R. H., 1978: Characteristic structure and growth of the non-precipitating cumulus layer over South Florida. Month. Weath. Rev. **106,** 1495-1504

KAHN, P. H. and J. A. BUSINGER, 1979: The effect of radiative flux divergence on entrainment of a saturated convective boundary layer. Quart. J. Roy. Met. Soc. 105, 303-306

KRAUS, E. B., 1963: The diurnal precipitation change over the sea. J. Atmos. Sei. 20, 551—556

KRAUS, H. and E. SCHALLER, 1978: A note on the closure in Lillytype inversion models. Tellus 30, 284—288

KRUEGERMEYER, L., 1975: Vertikale Transporte von Impuls, sensibler und latenter Wärme aus Profilmessungen über dem tropischen Atlantik während APEX. Ber. Inst. Radiomet. Mar. Met. Univ. Hamburg 29, pp. 84

KUHLBRODT, E. und J. REGER, 1933: Die aerologischen Methoden und das Beobachtungsmaterial. Wiss. Erg. Atl. Exp. "METEOR" 1925-27, Bd. 15

LeMONE, M. A. and W. T. PENNELL, 1975: The relationship of trade wind cumulus distribution to subcloud layer fluxes and structure. Month. Weath. Rev. **104,** 524-539

LILLY, D. K., 1968: Models of cloud-topped mixed layers under a strong inversion. Quart. J. Roy. Met. Soc. **94,** 292-309

LIST, R. J., 1956: Smithsonian Meteorological Tables. Smithsonian Inst. Press, Washington, D.C.

MAHRT, L., 1979: Penetrative convection at the top of a growing boundary layer. Quart. J. Roy. Met. Soc. **105,** 469-485

MALKUS, J. S., 1958: On the structure of the trade wind moist layer. Pap. Phys. Ocean. Met. M I II and Woods Hole Ocean Inst. Vol. 13, Nr. 2, 1-48

NEIBURGER, M., D. S. JOHNSON and C. CHIEN, 1961: Studies of the structure of the atmosphere over the eastern Pacific Ocean in summet. 1. The inversion over the eastern North Pacific Ocean. Univ. California Press, 94 pp.

NITTA, T. N. and S. ESBENSEN, 1974: Heat and moisture budget analysis using BOMEX data. Month. Weath. Rev. 102, 17-28

POND, S., G. T. PHELPS and J. E. PAQUIN, 1971: Measurements of turbulent fluxes of momentum, moisture and sensible heat over the ocean. J. Atmos. Sei. 28, 901-917

PRUEMM, D., 1976: Periodic and aperiodic variations of temperature, humidity and water temperature at the tropical Atlantic during ATEX. "Meteor" Forsch.-Ergeb. B11, 78-93

RIEHL, H., T. C. YEH, J. S. MALKUS and N. E. La SEUR, 1951 : The north-east trade of the Pacific Ocean. Quart. J. Roy, Met. Soc. 77, 598—626

RIEHL, H. and D. SOLTWICH, 1974: On the depth of the friction layer and the vertical transport of momentum in the trades. Beitr. Phys. Atmosph. 47, 56-66

SOMMERIA, G., 1976: Three-dimensional Simulation of turbulent processes in an ündisturbed trade wind boundary layer. J. Atmos. Sei. 33, 216-241

SOMMERIA, G. and J. W. DEARDORFF, 1977: Subgrid-scale condensation in models of non-precipitating clouds. J. Atmos. Sei. 34, 344-355

STULL, R. B., 1976: Mixed-layer depth model based on turbulent energetics. J. Atmos. Sei. 33, 1268-1278

TENNEKES, H., 1973: A model for the dynamics of the Inversion above a convective boundary layer. J. Atmos. Sei. 30, 558-567

TURNER, J. S., 1979: Buoyancy effects in fluids. Cambridge University Press, Cambridge

WAGNER, V., 1975: Zusammenhänge zwischen der troposphärischen Zirkulation und den energetischen Prozessen im Bereich der Hadleyzirkulation über dem Atlantik. Ber. Inst. Radiomet. Marit. Met. Univ. Hamburg, Nr. 26, 83 pp.

WARNER, J., 1977: Time Variation of updraft and water content in small cumulus clouds. I. Atmos. Sei. 34, 1306—1313

YANAI, M., S. ESBENSEN and J.-H. CHU, 1973: Determination of bulk properties of tropical cloud clusters from large scale heat and moisture budgets. J. Atmos. Sei. 30, 611-627